Partial Synchronization of Stochastic Oscillators through Hydrodynamic Coupling

Arran Curran,* Michael P. Lee, and Miles J. Padgett
School of Physics and Astronomy, SUPA, University of Glasgow, Glasgow G12 8QQ, United Kingdom

Jonathan M. Cooper
School of Engineering, University of Glasgow, Glasgow G12 8LT, United Kingdom

Roberto Di Leonardo
CNR-IPCF, UOS Roma, Dipartimento di Fisica, Università "Sapienza," I-00185 Roma, Italy
(Received 9 December 2011; published 13 June 2012)

Holographic optical tweezers are used to construct a static bistable optical potential energy landscape where a Brownian particle experiences restoring forces from two nearby optical traps and undergoes thermally activated transitions between the two energy minima. Hydrodynamic coupling between two such systems results in their partial synchronization. This is interpreted as an emergence of higher mobility pathways, along which it is easier to overcome barriers to structural rearrangement.

DOI: 10.1103/PhysRevLett.108.240601 PACS numbers: 05.40.−a, 05.45.Xt, 83.10.Pp, 87.80.Cc

Activated dynamics is ubiquitous in physics, chemistry, and biology [1,2]. Escape from a stable state occurs via transition events by which a system crosses an energy barrier, falling into a neighboring state. On the small length scales of colloidal particles and biological macromolecules, it is the surrounding fluid which provides the required fluctuations to overcome a barrier and, at the same time, the viscosity needed to relax the system in the second minimum by dissipating energy. With the addition of a spatial potential landscape consisting of two or more minima, such an environment allows a colloidal particle to undergo hops between the minima, provided that any energetic maximum is surmountable by thermal fluctuations [3–5]. Starting from a Fokker-Planck formulation of Brownian motion in bistable potentials, Kramers [1] was able to obtain an analytical expression for the hopping rates that depends solely on the local features of the underlying potential. McCann *et al.* [3] used two separate HeNe lasers to construct a bistable optical landscape where a 600 nm silica sphere was confined in a solvent fluid. The sphere hopped back and forth between the traps, providing the ideal representation of Kramers's ideas, and elegantly confirmed the link between hop rates and the features of the potential landscape. Since this first quantitative test of Kramers's theory, a number of experiments have been published investigating how the hop rates of stochastic oscillations behave under modulation of the potentials [6–10]. By asymmetrically modulating the depth of the potential wells and hence the phase between the forcing and the activated transitions, Simon and Libchaber [6] observed the synchronization of stochastic oscillations within a period equal to the mean Kramers time.

On this micron scale, both fluctuations and friction display long-range hydrodynamic correlations that inevitably couple the dynamics of suspended objects. For example, two colloidal particles in independent optical traps display correlations in their Brownian motions [11]. Whether the same hydrodynamic interaction could result in some degree of correlation in the thermally activated dynamics of nearby bistable systems is still an open and important question. Understanding how hydrodynamics can bias activated hops over energy barriers impacts the study of the slow dynamics of structural rearrangements in colloidal glasses and gels.

In this Letter, we use two colloidal spheres trapped in neighboring but separate bistable optical landscapes to reveal a significant difference between symmetric and antisymmetric simultaneous hops. While we measure a significant biasing, the total number of simultaneous hops transpires only to be that expected from two random oscillators. This is due to the stochastic nature of our oscillators, whose dynamics are driven by thermal fluctuations alone. We show that the difference between the number of symmetric and antisymmetric hops reduces as the inverse separation between the two systems, showing that the strength of the phenomenon scales with first order in the hydrodynamic coupling.

Sculpting of the bistable optical landscape is achieved by a holographic phase element generated by a gratings and lenses algorithm [12,13]. Holograms are imaged at the back aperture of a Carl Zeiss ×100 1.3 NA oil-immersion microscope objective and focused into a multispot array located at the focal plane (Fig. 1). Each bistable potential is constructed by having two individual focal spots placed in close proximity, such that a surmountable barrier forms between the two traps. We create two bistable potentials separated by a distance s, which is also controlled holographically. Care is taken to maintain symmetric bistable potentials by adjusting the optical intensities of each trap. Stilgoe *et al.* have recently given a report on the complexity of creating optical potentials using two optical traps [14]. Our samples are prepared with silica spheres (of

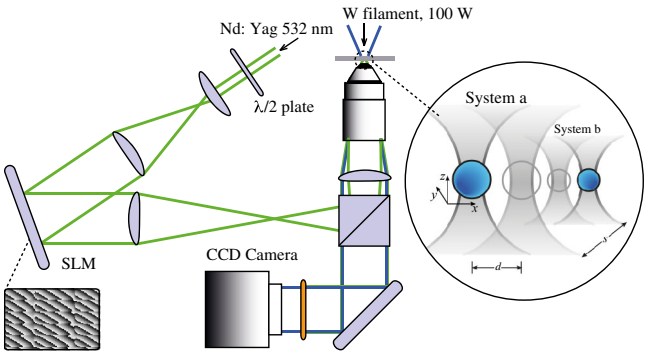

FIG. 1 (color online). Holographic optical tweezers. A spatial light modulator (SLM) is used to generate multiple traps at the focal plane of the ×100 oil-immersion microscope objective. Silica spheres are trapped with a frequency-doubled Nd:Yag laser, 5 μm above the cover slip. The left inset shows the hologram used to landscape two side-by-side bistable potentials. A schematic of the two optically trapped spheres in independent bistable potentials is shown in the inset on the right.

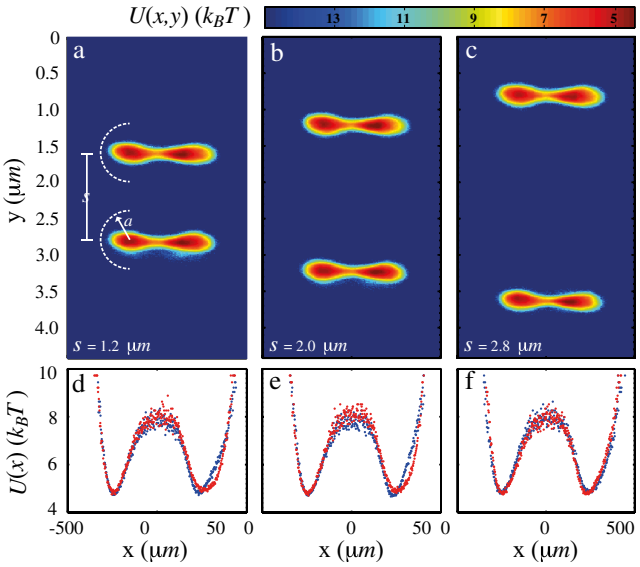

FIG. 2 (color online). Optical potential landscapes experienced by two 800 nm silica spheres. Potential energy distributions are recovered from particle trajectories, $x(t)$ and $y(t)$, as described in the text. The data are binned into bins of size 10 nm^2 for (a)–(c) and 2 nm for (d)–(f).

radius $a = 0.4$ μm, Bangs Laboratories) in deionized, distilled water with a 1:10^6 ratio. When preparing our samples, we add a weak saline solution just before sealing, so that any free debris is immobilized on the cover slip due to the reduced Debye length [15] while still allowing enough time to capture the two spheres required for the experiment. Sample cells are constructed with a single concave microscope slide (concave depth = 500 μm) and a square cover slip (thickness number 1.5), sealed with UV-curing optical adhesive. Using a few mW of frequency-doubled Nd:Yag laser light (532 nm), the trap stiffness in each trap is set at $\sim$1 pN/μm^{-1}. A Prosilica GE650 camera, operating at a frame rate of 1.55 kHz, is used to track the position of the spheres in the $x - y$ plane. Using a center-of-mass algorithm, these in-plane displacements are measured with nm precision [16]. Time series of the spheres' center of mass, $x(t)$ and $y(t)$, are extracted in blocks of 10^5 frames and accumulated for a total time period of 2–3 hours, significantly longer than the average between hops, which is of the order of 1 s.

Since the sampling rate is much greater than the corner frequency in the power spectrum of particle fluctuations, $f_c \sim 20$ Hz, the normalized histogram of particle positions $\rho(x, y)$ provides a direct measurement of the Boltzmann distribution, $\rho(x, y) = Z^{-1} \exp[-U(x, y)/k_B T]$, where k_B, T, and Z are, respectively, the Boltzmann constant, the temperature of the surrounding fluid, and the normalization constant. By inverting $\rho(x, y)$, we can directly access the underlying optical potential in units of $k_B T$ [Figs. 2, 3(b), and 3(d)].

The obtained potentials are shown in Figs. 2(a)–2(c) for three separations, $s = 1.2$, 2.0, and 2.8 μm. The potentials along the hopping axis for system a [dark gray (blue) ○'s] and system b [light gray (red) ○'s], presented in Figs. 2(d)–2(f), confirm that the optical landscapes of each system are not significantly perturbed as they approach. It is worth noting that, although the optical landscape is made of two optical traps whose centers are separated by 800 nm, the separation between the minima of the obtained bistable potential is only $d \sim 400$ nm. This is due to the sphere experiencing restoring forces from both optical traps, leading to an offset in the equilibrium position in each individual trap and shortening the hopping distance.

Figures 3(a) and 3(c) show a 10 s sample trace of particle position on the x axis (the axis along which hopping occurs) taken at large separation, $s = 3.6$ μm. The corresponding potentials are given in Figs. 3(b) and 3(d). A single-particle power spectrum is shown in Fig. 3(e) for the shortest separation, $s = 1.2$ μm. Two separated time scales are visible, a low frequency component describing the hopping dynamics and a high frequency component describing the fluctuations around the local minima. For an isolated hopping system, the Fourier amplitude, $\hat{x}(\nu)$, of the particle's x position will be distributed with a double Lorentzian spectrum,

$$\langle \hat{x}^*(\nu)\hat{x}(\nu)\rangle = \frac{k_B T}{\pi k}\frac{f_c}{\nu^2 + f_c^2} + \frac{d^2}{4\pi}\frac{2f_h}{\nu^2 + (2f_h)^2}. \quad (1)$$

The first term is the standard spectrum for a bead of mobility $m_0 = 1/(6\pi\eta a)$ (where $\eta = 1$ m Pa s is taken as the viscosity) in an optical trap of strength k, and thus, a corner frequency given by $f_c = m_0 k/2\pi$. The second term describes hopping events over a distance d and a jump probability per unit time given by f_h. The hopping frequency can be anticipated using Kramers's theory

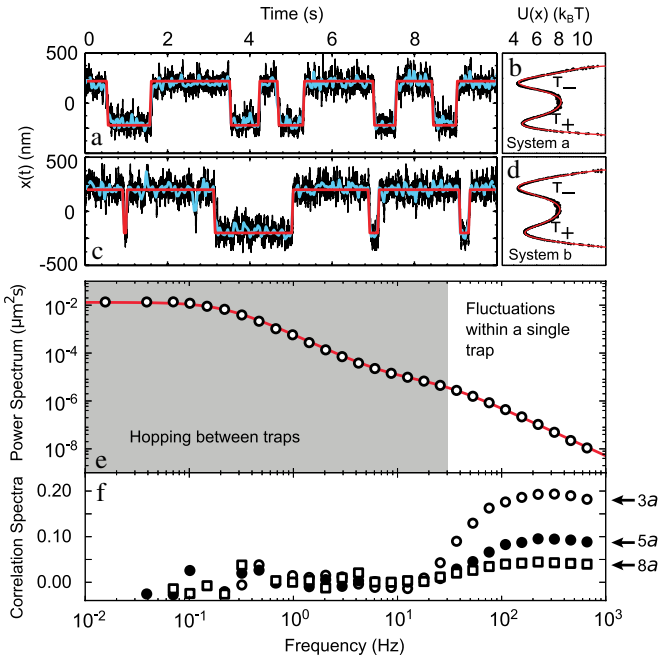

FIG. 3 (color online). (a),(c) 10 s sample of the spheres' position along the x axis (black line) for each system separated by $s = 3.6$ μm. The block filtered [light gray (blue) line] and digitized traces [dark gray (red) line] are also shown. (b), (d) Corresponding potentials (black ○'s) with fitted polynomials (red line). (e) Single-particle power spectrum for $s = 1.2$ μm, along with a double Lorentzian fit, as discussed in the text. (f) Correlation spectra for three separations, evidencing hydrodynamic correlations in the high frequency region.

$f_h = \omega_0 \exp[-\Delta U/k_B T]$, where ΔU is the height of the potential barrier and the prefactor $\omega_0 = m\sqrt{\kappa_i \kappa_s}$ depends on the particle mobility m_0 and on the curvatures of the underlying potential at the stationary points $\kappa_{i,s} = |\partial^2 U/\partial x^2|_{x=x_{i,s}}$. Knowing the temperature, viscosity, and particle radius means that all remaining parameters can be directly evaluated from the features of the stationary points in the obtained potential energy. The resulting curve is shown as a solid line in Fig. 3(e) and fits the measured power spectrum well. Searching for hydrodynamic correlations, we plot in Fig. 3(f) the correlation spectra $\langle \hat{x}_a^*(\nu)\hat{x}_b(\nu)\rangle$ normalized by the average single-particle power spectra $(1/2)\sum_{\alpha=a,b}\langle \hat{x}_\alpha^*(\nu)\hat{x}_\alpha(\nu)\rangle$. A marked positive correlation at high frequencies gets larger as the two systems approach. This is the well-known phenomenon by which the mobility of rigid motions is higher than that for relative motions, so that at short times the particles tend to move collectively [11]. However, at low frequencies dominated by hopping dynamics, no sign of correlation is observable even when the two systems are close together.

Despite the lack of any obvious sign of collective motion in the low frequency correlations spectrum [Fig. 3(f)], further analysis of our data reveals a significant correlation. Rather than averaging the correlation over all points, we examine only the instances where both particles hop at the same time, either in the same direction (symmetric) or the opposite direction (antisymmetric). To examine these instances, we first average the position time series in blocks of 60 frames [Figs. 3(a) and 3(c), light gray (blue) line]. This acts as a low pass filter with a cutoff frequency of about 25 Hz, just higher than the trap corner frequency, filtering out the fast dynamics of fluctuations during a hop. The blocked data are then digitized into a two-state variable $\bar{x}(t) \in -1, +1$, denoting the left and right states of the bistable potential [Figs. 3(a) and 3(c), dark gray (red) line]. For each system, we then extract a time series of hop events from $-1 \rightarrow +1$ and $+1 \rightarrow -1$. These data represent a cumulative acquisition of 215 minutes at 1550 Hz, with $\sim 10^4$ transition events. The distributions of intervals between hops are fitted with an exponential decay, yielding the characteristic dwell time for each state. These measured dwell times are consistent with Kramers's formula applied to the detailed shape of the underlying potential. Each bistable potential is fitted with an eighth-order polynomial [Figs. 3(b) and 3(d), red line], the second derivative of which gives the Kramers prefactor term ω_0 when evaluated at the stationary points. Numerical results of ω_k^{-1} are given in the third column of Table I. The dwell times are measured from $x(t)$, the mean of which are given in the second column. The probability distribution of the dwell times is fitted with an exponential decay, giving the first column in Table I.

Each transition event is assigned a duration of one blocked sequence of frames, $\delta t = 39$ ms. We count the number of occurrences of possible coincident events, namely, p and n, where we define a p coincident as having occurred when both spheres hop in the same direction and an n coincidence when both spheres hop in opposite directions. Figure 4(a) shows this nomenclature. It is expected that two uncoupled stochastic oscillators will show a finite number of coincidences, $\langle N\rangle$, depending on the observed time period, T, and the temporal window, δt, in which we define a coincidence and the transition rates of the two oscillators, $\tau_{a,b}^{-1}$, given by

$$\langle N\rangle = \delta t T(\tau_a \tau_b)^{-1}. \quad (2)$$

TABLE I. Characteristic dwell times for each individual potential obtained by exponential fitting to the probability distributions of the states' dwell times, along with the mean value of raw dwell times and from Kramers's formula. All numbers are in units of s.

	Fit	Mean	ω_k^{-1}
System a	0.54	0.57	0.46
	0.66	0.68	0.62
System b	0.48	0.50	0.37
	0.74	0.73	0.61

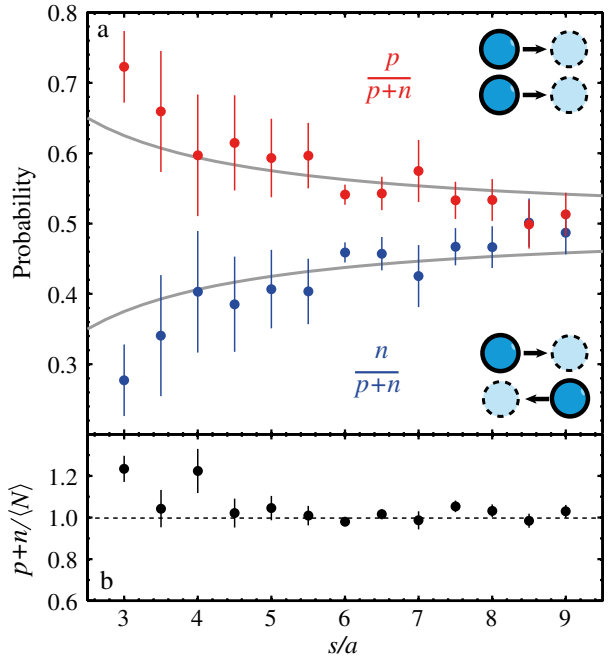

FIG. 4 (color online). (a) Probability of coincidences over a range of system separations s. p and n coincidences are defined by the inset cartoons. Coincidence events are counted as described in the text and presented as light gray (red) ○'s for p and dark gray (blue) ○'s for n. Data are normalized by $p + n$. The solid lines represent the splitting in p and n, assuming a linear dependence on hydrodynamic coupling with a strength of $3a/4s$. (b) The total counted coincidences at each system separation normalized by the expected number, $\langle N\rangle$ [Eq. (2)], with an error of $\pm\sqrt{p+n}/\langle N\rangle$.

For two uncoupled stochastic oscillators, we expect an equal probability for symmetric and antisymmetric simultaneous hops ($p = n$). Figure 4(a) shows the measured probabilities of p and n coincidences occurring over a range of system separations. With the two systems placed in close proximity to each other ($s \sim 3a$), the probability of observing a p coincidence is significantly greater than observing an n coincidence ($p - n > \langle N\rangle^{-1/2}$). At increasing separations, both p and n coincidence probabilities approach 0.5, ruling out the possibility that the synchronization could be ascribed to asymmetries in the optical landscapes. We note that the total number of observed coincidences, $(p + n)/\langle N\rangle$, is unchanged with separation [Fig. 4(b)]. Coming back to Kramers's formula for a single-particle hopping rate, we notice that particle mobility appears as a prefactor to an energetic activation term. We may then conjecture that the rates of symmetric hops and antisymmetric hops have a similar form with an activation term and a prefactor that would also depend, respectively, on the collective and relative mobilities [17–19]. Moreover, the splitting between p and n seems to decay with distance, as is the case for hydrodynamic splitting between collective and relative mobilities, as shown by the $0.5 \pm (3/4)(a/s)$ lines in Fig. 4(a).

In conclusion, the thermally activated jumps of two 800 nm silica spheres in neighboring bistable optical landscapes are shown to be coupled via hydrodynamic interactions. Because of the higher mobility of collective motions, when two systems are in close proximity, there is a higher probability of observing a symmetric hop, while antisymmetric hops are less common. We argue that the experimental environment studied here provides an idealized representation of interacting stochastic oscillations that occur in nature. It will be interesting to extend the present study to a larger ensemble of bistable systems. For example, looking for the emergence of more complex, cooperatively rearranging regions could aid the understanding of the role of hydrodynamic interactions in the glassy dynamics of concentrated colloidal suspensions [20].

*arran.curran@glasgow.ac.uk

[1] H. A. Kramers, Physica (Amsterdam) **7**, 284 (1940).
[2] P. Hänggi, P. Talkner, and M. Borkovec, Rev. Mod. Phys. **62**, 251 (1990).
[3] L. I. McCann, M. Dykman, and B. Golding, Nature (London) **402**, 785 (1999).
[4] J. Kotar, M. Leoni, B. Bassetti, M. C. Lagomarsino, and P. Cicuta, Proc. Natl. Acad. Sci. U.S.A. **107**, 7669 (2010).
[5] R. Benzi, A. Sutera, and A. Vulpiani, J. Phys. A **14**, L453 (1981).
[6] A. Simon and A. Libchaber, Phys. Rev. Lett. **68**, 3375 (1992).
[7] V. N. Smelyanskiy, M. I. Dykman, and B. Golding, Phys. Rev. Lett. **82**, 3193 (1999).
[8] J. Lehmann, P. Reimann, and P. Häanggi, Phys. Rev. Lett. **84**, 1639 (2000).
[9] R. S. Maier and D. L. Stein, Phys. Rev. Lett. **86**, 3942 (2001).
[10] Y. Seol, D. L. Stein, and K. Visscher, Phys. Rev. Lett. **103**, 050601 (2009).
[11] J. C. Meiners and S. R. Quake, Phys. Rev. Lett. **82**, 2211 (1999).
[12] J. Liesener, M. Reicherter, T. Haist, and H. J. Tiziani, Opt. Commun. **185**, 77 (2000).
[13] J. Leach, K. Wulff, G. Sinclair, P. Jordan, J. Courtial, L. Thomson, G. Gibson, K. Karunwi, J. Cooper, Z. J. Laczik, and M. Padgett, Appl. Opt. **45**, 897 (2006).
[14] A. B. Stilgoe, N. R. Heckenberg, T. A. Nieminen, and H. Rubinsztein-Dunlop, Phys. Rev. Lett. **107**, 248101 (2011).
[15] C. Alvarez and G. Tellez, J. Chem. Phys. **133**, 144908 (2010).
[16] G. M. Gibson, J. Leach, S. Keen, A. J. Wright, and M. J. Padgett, Opt. Express **16**, 14 561 (2008).
[17] E. R. Dufresne, T. M. Squires, M. P. Brenner, and D. G. Grier, Phys. Rev. Lett. **85**, 3317 (2000).
[18] A. Curran, A. M. Yao, G. M. Gibson, R. Bowman, J. M. Cooper, and M. J. Padgett, J. Biophoton **3**, 244 (2010).
[19] J. Happel and H. Brenner, *Low Reynolds Number Hydrodynamics* (Kluwer, Dordrecht, 1983).
[20] E. R. Weeks, J. C. Crocker, A. C. Levitt, A. Schofield, and D. A. Weitz, Science **287**, 627 (2000).